



Structural MRI Reveals Cervical Spinal Cord Atrophy in the P301L Mouse Model of Tauopathy: Gender and Transgene-Dosing Effects

Thomas Sartoretti^{1†}, Robert P. Ganley^{2†}, Ruiqing Ni^{1,3}, Patrick Freund^{3,4}, Hanns Ulrich Zeilhofer^{2,3,5} and Jan Klohs^{1,3*}

¹Institute for Biomedical Engineering, ETH & University of Zurich, Zurich, Switzerland, ²Institute of Pharmacology and Toxicology, University of Zurich, Zurich, Switzerland, ³Zurich Neuroscience Center (ZNC), Zurich, Switzerland, ⁴Balgrist University Hospital, University of Zurich, Zurich, Switzerland, ⁵Institute for Pharmaceutical Sciences, ETH Zurich, Zurich, Switzerland

OPEN ACCESS

Edited by:

Stephen D. Ginsberg,
Nathan Kline Institute for Psychiatric
Research, United States

Reviewed by:

Shu-Wei Richard Sun,
Loma Linda University, United States
Xihong Lu,
Shanghai University of Medicine and
Health Sciences, China

*Correspondence:

Jan Klohs
klohs@biomed.ee.ethz.ch

[†]These authors have contributed
equally to this work and share first
authorship

Specialty section:

This article was submitted to
Alzheimer's Disease and Related
Dementias,
a section of the journal
Frontiers in Aging Neuroscience

Received: 30 November 2021

Accepted: 24 March 2022

Published: 02 May 2022

Citation:

Sartoretti T, Ganley RP, Ni R,
Freund P, Zeilhofer HU and Klohs J
(2022) Structural MRI Reveals
Cervical Spinal Cord Atrophy in the
P301L Mouse Model of Tauopathy:
Gender and Transgene-Dosing
Effects.
Front. Aging Neurosci. 14:825996.
doi: 10.3389/fnagi.2022.825996

In primary tauopathies, the deposition of tau neurofibrillary tangles and threads as well as neurodegenerative changes have been found within the brain and spinal cord. While degenerative changes have been intensively studied in the brain using structural magnetic resonance imaging (MRI), MRI studies investigating the spinal cord are still scarce. In the present study, we acquired *ex vivo* high resolution structural MRI of the cervical spinal cord of 8.5–9 month old hemizygous and homozygous P301L mice and non-transgenic littermates of both genders. We assessed the total cross-sectional area, and the gray and white matter anterior-posterior width and left-right width that are established imaging marker of spinal cord degeneration. We observed significant tissue-specific reductions in these parameters in female P301L mice that were stronger in homozygous than in hemizygous P301L mice, indicating both an effect of gender and transgene expression on cervical spinal cord atrophy. Moreover, atrophy was stronger in the gray matter than in the white matter. Immunohistochemical analysis revealed neurodegenerative and neuroinflammatory changes in the cervical spinal cord in both the gray and white matter of P301L mice. Collectively, our results provide evidence for cervical spinal cord atrophy that may directly contribute to the motor signs associated with tauopathy.

Keywords: tau, spinal cord, magnetic resonance imaging, frontotemporal dementia, Alzheimer's disease, animal models

INTRODUCTION

Primary tauopathies are characterized by the aggregation of insoluble, hyperphosphorylated tau protein into intraneuronal neurofibrillary tangles, threads, and inclusions in neurons and glia (Lee et al., 2001). This group includes progressive supranuclear palsy, corticobasal degeneration, and a number of sporadic and familial frontotemporal dementias and Alzheimer's disease,

that ketamine acts on postsynaptic neurons where beta-amyloid is also deposited into extracellular plaques in addition to tau (Grundke-Iqbal et al., 1986). In healthy neurons, the tau protein stabilizes axonal microtubules that are necessary for proper neuronal function, but in Alzheimer's disease and tauopathies, there is an abnormal accumulation of tau protein in somatodendritic compartments, associated with axonal and synaptic dysfunction, neuronal loss, atrophy, and cognitive decline (Lee et al., 2001). Tauopathy spreads sequentially across the brain, through neuroanatomically and functionally connected areas (Braak and Braak, 1991; Vogel et al., 2020).

Tauopathy is also known to extend into the spinal cord (SC). Neuropathological studies have shown that the SC of patients with Alzheimer's disease and variants of the disease have tau neurofibrillary tangles and threads in the SC (Schmidt et al., 2001; Rudzinski et al., 2008; Dugger et al., 2013). Neuropathological findings were most pronounced in the cervical SC, with a progressive decrease at the thoracic and lumbar level (Dugger et al., 2013). In addition, there is marked degeneration of the corticospinal tract with myelin damage and gliosis (Verkkoniemi et al., 2001; Rudzinski et al., 2008). Furthermore, Alzheimer's disease and tauopathy patients have, in addition to cognitive impairment, characteristic motor signs, including motor slowing, rigidity, gait and posture abnormalities, bradykinesia and tremor, which are related to worsened clinical outcome (Scarmeas et al., 2005; Waite et al., 2005; Josephs, 2017). Related studies in animal models of tauopathy have shown the deposition of phosphorylated tau and neurofibrillary tangles in the SC in several different strains (Ishihara et al., 1999; Spittaels et al., 1999; Duff et al., 2000; Probst et al., 2000; Götz et al., 2001; Allen et al., 2002; Higuchi et al., 2002; Lin et al., 2003, 2005; Zehr et al., 2004; Yoshiyama et al., 2007). Moreover, these studies provided evidence for neuronal degeneration, myelin damage, and inflammation. The SC pathology was accompanied by motor signs such as paresis, tremor, and muscle weakness (Duff et al., 2000; Probst et al., 2000; Allen et al., 2002; Higuchi et al., 2002; Lin et al., 2005). Thus, the SC is a clinical eloquent site in the pathology and symptomatology of tauopathies.

High-resolution structural magnetic resonance imaging (MRI) is widely applied in clinical studies to assess degenerative changes of the brain (Klohs and Rudin, 2011). Such studies revealed distinct pattern of gray and white matter atrophy in the brain of patients with progressive supranuclear palsy (Price et al., 2004), corticobasal degeneration (Tokumaru et al., 2009), Pick's disease (Lieberman et al., 1998), frontotemporal dementia (Ghetti et al., 2008; Rohrer et al., 2010), and Alzheimer's disease (Holland et al., 2009; Shi et al., 2009; Tabatabaei-Jafari et al., 2019; Lorenzi et al., 2020). Importantly, regional atrophy is detectable in longitudinal studies within short time intervals (Holland et al., 2009; Rohrer et al., 2010), is a marker of cognitive decline (Tabatabaei-Jafari et al., 2019), and distinguish between different tauopathies and other causes of neurodegeneration (Price et al., 2004; Ghetti et al., 2008; Shi et al., 2009; Tokumaru et al., 2009; Rohrer et al., 2010). Related MRI studies in animal

models of tauopathies have also revealed cerebral atrophy, for example atrophy was found in the hippocampus and cortex in the rTg4510 tau mouse model (Xie et al., 2010; Yue et al., 2011; Holmes et al., 2017; Ma et al., 2019).

Despite the involvement of the SC in tau pathology, structural MRI studies of the SC in patients and animal models are still scarce. A recent study has reported atrophy of the cervical SC in Alzheimer's disease patients (Lorenzi et al., 2020). The study reported reduced cross-sectional areas of C1 to C5 and reduced cross-sectional volumes in C1 and C2. However, the tau pathology has been identified as a major driver of local neurodegeneration in Alzheimer's disease (Iaccarino et al., 2018; Joie et al., 2020). This has prompted us to investigate morphological changes in the cervical SC in the P301L mouse model of four-repeat tauopathy (Götz et al., 2001). We acquired *ex vivo* high-resolution structural MRI data of the cervical SC of 8.5–9 months old P301L mice and non-transgenic littermates and assessed morphometric metrics, that are established imaging markers of SC degeneration (Mann et al., 2007; Ellingson et al., 2010; Seif et al., 2018). To test for transgene-dose-dependent effects, we assessed morphometric metrics for both hemizygous and homozygous P301L mice and compared them to non-transgenic littermates. We hypothesized that effects on morphometric parameters would be stronger in homozygotes than in hemizygotes, because of the stronger tau transgene expression in homozygous P301L mice. Moreover, given the reported effects of gender on tau pathology in animal models of tauopathy (Yue et al., 2011; Sun et al., 2020), we examined the effect of gender on the measured morphological parameters of the cervical SC.

MATERIALS AND METHODS

Animal Model

P301L mice expressing the human four-repeat tau isoform under control of the murine Thy 1.2 promoter were backcrossed with C57BL/6J mice for >20 generations and maintained on a C57BL/6J background [B6.Dg-Tg(Thy1.2-TauP301L)183 Nitsch] (Götz et al., 2001). The strain expresses the human four-repeat tau isoform along with human pathogenic mutation P301L under the neuronal Thy 1.2 promoter. P301L mice show high expression of human P301L tau in neurons and show abnormal filaments of phosphorylated tau in the cortex, hippocampus, and SC in an age-dependent fashion (Götz et al., 2001; Ni et al., 2020). Hemizygous P301L mice were used for breeding to generate homozygous P301L mice. All mice were maintained under specific pathogen-free conditions. Animals were housed in ventilated cages inside a temperature-controlled room (22°C, 50% air humidity), under a 12-h dark/light cycle. Each cage housed up to five mice. Paper tissue and red Tecniplast mouse house® (Tecniplast, Milan, Italy) shelters were placed in cages as environmental enrichments. Pelleted food (3437PXL15, CARGILL) and acidified water were provided *ad libitum*.

Sample Preparation

All experiments were performed in accordance with the Swiss Federal Act on Animal Protection and were approved by the Cantonal Veterinary Office Zurich (permit number: ZH044/19). All animal experiments are reported in compliance with the ARRIVE 2.0 guidelines. A total of eight male and eight female hemizygous, eight male and seven female homozygous P301L mice and eight male and nine female non-transgenic littermates between 8.5 and 9 months of age were used. Mice were intracardially perfused under deep anesthesia with sodium pentobarbital (100 mg/kg body weight). Mice were perfused intracardially with 10 ml of 0.1 M phosphate buffered saline (PBS) followed by 4% paraformaldehyde in 0.1 M PBS (pH 7.4). Whole vertebral columns were dissected and post-fixed in 4% paraformaldehyde in 0.1 M PBS (pH 7.4) for 6 days and stored in 0.1 M PBS at 4°C thereafter until usage. Samples were placed in a 20 ml syringes filled with perfluoropolyether (Fomblin Y, LVAC 16/6, average molecular weight 2,700, Sigma-Aldrich, USA).

Magnetic Resonance Imaging Protocol

Data were acquired on a 7/16 small animal MR Pharmascan (Bruker BioSpin AG, Ettlingen, Germany) equipped with an actively shielded gradient set of 760 mT/m and 80 μ s rise time, operated by a Paravision 6.0 software platform (Bruker BioSpin). A transmit/receive quadrature birdcage coil with an inner diameter of 23 mm (Bruker BioSpin AG) was used.

First, a T_2 -weighted Turbo Spin Echo sequence was acquired with 10 slices, field-of-view of 20 mm \times 10 mm, matrix dimension 256 \times 128, with a nominal voxel resolution of 78 μ m \times 78 μ m was acquired for anatomical orientation and geometrical planning. Imaging parameters were: repetition time of 1,500 ms, an echo time of 6 ms, 2 averages, and a RARE factor of 4 in an acquisition time of 1 min 12 s. Then, T_1 -weighted structural images were acquired with a 3D fast low angle shot (FLASH) sequence with a field of view of 20 mm \times 20 mm \times 10 mm, matrix dimension of 400 \times 400 \times 200, resulting in a nominal voxel resolution of 50 μ m \times 50 μ m \times 50 μ m. In some cases, two field-of-views were acquired to cover the area of interest (C1-C6). The following imaging parameters were chosen: a repetition time of 50 ms, an echo time of 10 ms, 10 averages, within a total scan time of 12 h and 12 min (1 field-of-view) or 24 h and 24 min (2 field-of-views). A field map was acquired with a field-of-view of 15 mm \times 15 mm \times 15 mm, matrix dimensions of 64 \times 64 \times 64 to give a resolution of 234 μ m \times 234 \times 234 μ m, repetition time 20 ms, echo time 2 ms, 8 averages, within an acquisition time of 10 min 55 s, for using the MAPSHIM protocol for shimming. Field-of-view suppression was used to eliminate signal from regions outside the field-of-view.

Image Analysis

MR images were analyzed in a validated, open-source, FDA-approved medical imaging program (Osirix MD, v12.0, Geneva, Switzerland; Rosset et al., 2004) by a person blinded to the genotype and gender. Upon inspection of sagittal and coronal image reformations and by using an anatomical atlas (Watson et al., 2009) for guidance, representative axial T_1 -weighted

image slices matching C1–C6 SC segments were identified (Figure 1). For each SC segment, three to four consecutive and representative axial image slices were considered for further analysis. Specifically, using freehand region-of-interest (ROI) measurements, the total cross-sectional area, and the gray and white matter anterior-posterior width and left-right width were measured for a given axial slice by manually outlining relevant anatomical structures. The values were subsequently averaged across all three (or four) axial slices, thus rendering a single score per measurement category and SC segment for a given mouse.

Immunohistochemistry

For immunohistochemistry, three female hemizygous, three female homozygous P301L mice and three female non-transgenic littermates were analyzed. Fixed tissues were cryoprotected in 30% w/v sucrose dissolved in a 0.1 M sodium phosphate buffer for 24–72 h at 4°C. Following cryoprotection, SCs were dissected and the cervical enlargement of each was embedded in Neg-50 freezing medium at –20°C. SCs were embedded upright to allow transverse sections to be taken. Embedded SCs were mounted on a freezing microtome (Hyrax KS-34) and were sectioned at 60 μ m with a sliding blade (Zeiss S-30). SC sections were either stored in antifreeze solution, containing 50 mM sodium phosphate buffer, 30% ethylene glycol, 15% glucose, and sodium azide (200 mg/L), or processed directly for immunostaining.

Sections were rinsed three times in 0.1 M PB for 10 min, followed by a 30 min incubation in 50% ethanol. Sections were then rinsed three times for 10 min each with PBS containing extra salt (8 g NaCl per liter PBS), before being incubated for 2 days at 4°C in primary antibodies against NeuN and ionized calcium-binding adapter molecule 1 (Iba-1) to label neurons and resident microglia respectively (primary antibodies suspended in PBS extra salt, 10% v/v normal donkey serum, 0.3% v/v Triton-X). The sections were then rinsed three times for 10 min each in PBS extra salt before being incubated overnight at 4°C in species specific secondary antibodies (suspended in PBS extra salt with 0.3% v/v Triton-X). The following day the tissues were rinsed three times in PBS extra salt, counterstained with DAPI, and mounted on microscope slides in DAKO antifade mounting medium. A list of antibodies used in this study can be found in Table 1.

Confocal Image Acquisition and Image Analysis

All images were acquired on a Zeiss lsm 800 microscope with Zen blue software. Image stacks were taken with 5 μ m z-spacing through a 20 \times oil immersion objective lens up to a depth of 20 μ m from the surface of the section. For analysis, a tile scan was taken to encompass all white and gray matter from the dorsal and ventral horns for half of the SC (hemisection). For all experiments, identical scan settings were used, such as laser power, digital gain, and image resolution. Orthogonal z-projections were produced for each image (four confocal scans at 5 μ m z-spacing), which were then analyzed using ImageJ.

Image projections were imported into ImageJ and the gray matter and white matter were delineated using the area or NeuN and dense DAPI staining to identify the gray matter. Mean pixel

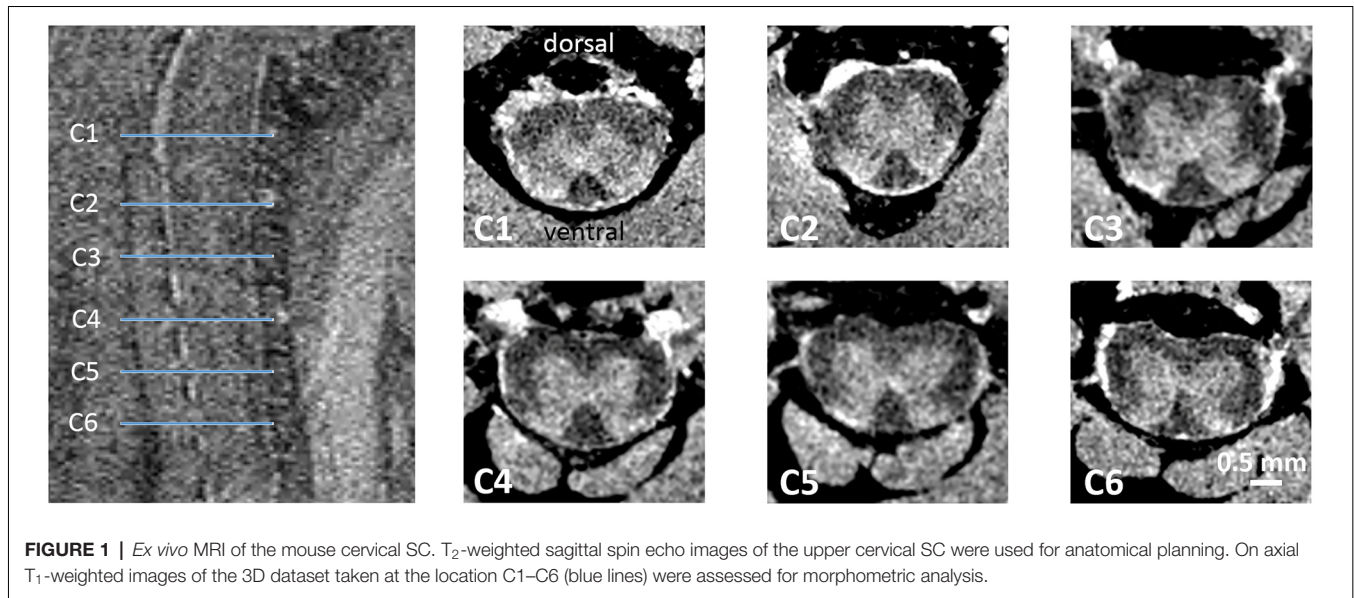


FIGURE 1 | Ex vivo MRI of the mouse cervical SC. T₂-weighted sagittal spin echo images of the upper cervical SC were used for anatomical planning. On axial T₁-weighted images of the 3D dataset taken at the location C1–C6 (blue lines) were assessed for morphometric analysis.

TABLE 1 | List of primary and secondary antibodies used in this study.

Antibody	Host	Supplier/Source	Cat#/RRID	Dilution
NeuN	Guinea pig	Synaptic systems	266004/AB_2619988	1:1,000
Iba-1	Rabbit	Wako	019-19741/AB_839504	1:2,000
Guinea pig-A647	Donkey	Jackson ImmunoResearch Laboratories	706-469-148/-	1:500
Rabbit	Donkey	Jackson ImmunoResearch Laboratories	711-546-152/AB_2340619	1:500

intensities were measured for the gray and white matter for NeuN and Iba-1 staining, and the size of each of these areas was determined. Between three and four sections were analyzed for each animal ($n = 3$ per group).

Statistical Analysis

For assessing anatomical variation and effect of gender on morphometric metrics, we performed a two-way ANOVA with segments and gender as independent variables and cross-sectional areas, gray matter area and white matter area as dependent variable. *Post hoc* analysis (Holm-Sidak method) was used to assess interaction between groups. Comparisons of immunohistochemical stainings between group means were made using a one-way ANOVA with Bonferroni *post hoc* correction for multiple comparisons.

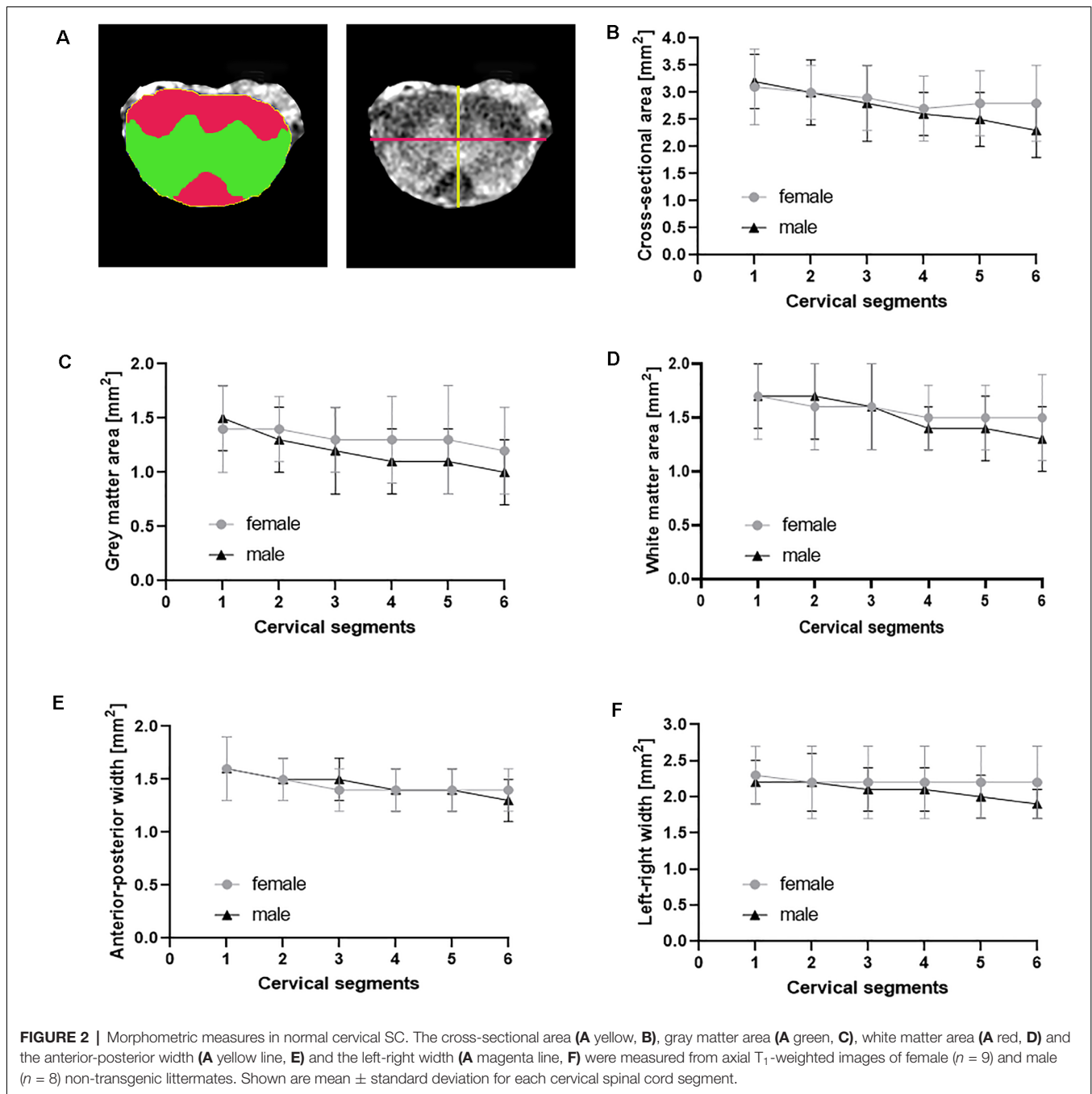
RESULTS

Morphometric Measurements in the Normal Cervical Cord

We first assessed morphometric metrics of the normal cervical SC in non-transgenic littermates (Figure 2, Table 2). Cross-sectional areas decreased from level C1 to C4 as described (Sengul and Watson, 2012). Similarly, gray matter and white matter areas decreased from segment C1 to C4. Values were starting to increase from C5 to C6, encompassing the cervical enlargement. Anterior-posterior and left-and right widths were decreasing from segment C1 to C6.

To test for effects of gender on the morphometric measures, we performed a two-way ANOVA with segment and gender as independent variables and morphometric parameters as a dependent variable. We found no statistically significant two-way interaction between gender and segments for the cross-sectional area, $F_{(5)} = 0.748$, $p = 0.589$. Subsequent analysis of main effects revealed no difference in the cross-sectional area between female and male non-transgenic littermates, $F_{(1)} = 1.917$, $p = 0.170$. A significant difference between cervical segments was found, $F_{(5)} = 2.790$, $p = 0.022$. *Post hoc* analysis showed only differences between C1 and C6, with a difference of the mean = 0.620, $t = 3.085$, $p = 0.040$. Furthermore, there was no statistically significant two-way interaction between gender and segments for gray matter area, $F_{(5)} = 0.683$, $p = 0.637$. Also there were no main effects of gender, $F_{(1)} = 3.086$, $p = 0.082$ or segment, $F_{(5)} = 2.251$, $p = 0.056$ on gray matter area. Similarly, there was no statistically significant two-way interaction between gender and segments for white matter area, $F_{(5)} = 0.520$, $p = 0.761$. No main effects of gender, $F_{(1)} = 0.347$, $p = 0.558$ or segments, $F_{(5)} = 1.895$, $p = 0.103$ was found.

Furthermore, there was no statistically significant two-way interaction between gender and segments for anterior-posterior width $F_{(5)} = 0.642$, $p = 0.668$. And there was no main effects of gender, $F_{(1)} = 0.101$, $p = 0.752$ or segments, $F_{(5)} = 2.195$, $p = 0.062$ on anterior-posterior width. Similarly, there was no statistically significant two-way interaction between gender and segments for left-right width $F_{(5)} = 0.396$, $p = 0.850$. No main effects of gender, $F_{(1)} = 1.718$, $p = 0.193$ or segments,



$F_{(5)} = 0.526$, $p = 0.756$ was found. Taken together, we did not find differences in the measured morphometric metrics between individual segments of the cervical SC at level 1–6 and no effect of gender on the measured cord metrics.

Effect of Tau Pathology on Cervical SC Cross-Sectional Area

We then compared the effect of tau pathology on the morphometric measures (Tables 2, 3). We compared total cross-sectional area between age-matched hemizygous, homozygous

P301L mice, and non-transgenic littermates. There was a statistically significant two-interaction between genotype and gender for total cross-sectional area, $F_{(2)} = 3.682$, $p = 0.026$. Subsequent analysis of the factor genotype between female animals revealed a significant difference between homozygous P301L mice and non-transgenic littermates, with a difference of the mean = 0.577, $t = 4.263$, $p < 0.001$. Cross-sectional areas were reduced across all cervical segments (Table 3). A significant difference between cross-sectional areas was also observed between homozygous and hemizygous P301L mice,

TABLE 2 | Morphometric measures.

Total cross-sectional area [mm ²]		C1	C2	C3	C4	C5	C6
NTL	Female	3.1 ± 0.7	3.0 ± 0.5	2.9 ± 0.6	2.7 ± 0.6	2.8 ± 0.6	2.8 ± 0.7
	Male	3.2 ± 0.5	3.0 ± 0.6	2.8 ± 0.7	2.6 ± 0.4	2.5 ± 0.5	2.3 ± 0.5
Hemizygote	Female	3.2 ± 0.5	2.9 ± 0.7	2.8 ± 0.7	2.6 ± 0.5	2.6 ± 0.7	2.5 ± 0.7
	Male	3.4 ± 0.7	3.1 ± 0.6	2.9 ± 0.6	2.8 ± 0.6	2.7 ± 0.5	2.7 ± 0.6
Homozygote	Female	2.8 ± 0.8	2.5 ± 0.8	2.3 ± 0.9	2.2 ± 0.9	2.1 ± 1.0	1.9 ± 0.9
	Male	2.9 ± 0.5	2.8 ± 0.5	2.7 ± 0.6	2.5 ± 0.6	2.5 ± 0.6	2.5 ± 0.5
Gray matter area [mm ²]		C1	C2	C3	C4	C5	C6
NTL	Female	1.4 ± 0.4	1.4 ± 0.3	1.3 ± 0.3	1.3 ± 0.4	1.3 ± 0.5	1.2 ± 0.4
	Male	1.5 ± 0.3	1.3 ± 0.3	1.2 ± 0.4	1.1 ± 0.3	1.1 ± 0.3	1.0 ± 0.3
Hemizygote	Female	1.5 ± 0.3	1.3 ± 0.3	1.2 ± 0.3	1.1 ± 0.3	1.1 ± 0.3	1.1 ± 0.4
	Male	1.7 ± 0.5	1.5 ± 0.3	1.3 ± 0.3	1.3 ± 0.4	1.2 ± 0.3	1.2 ± 0.4
Homozygote	Female	1.2 ± 0.4	1.0 ± 0.4	0.9 ± 0.4	1.0 ± 0.6	0.8 ± 0.5	0.8 ± 0.6
	Male	1.4 ± 0.4	1.3 ± 0.4	1.2 ± 0.4	1.3 ± 0.4	1.2 ± 0.4	1.2 ± 0.4
White matter area [mm ²]		C1	C2	C3	C4	C5	C6
NTL	Female	1.7 ± 0.4	1.6 ± 0.4	1.6 ± 0.4	1.5 ± 0.3	1.5 ± 0.3	1.5 ± 0.4
	Male	1.7 ± 0.3	1.7 ± 0.4	1.6 ± 0.4	1.4 ± 0.2	1.4 ± 0.3	1.3 ± 0.3
Hemizygote	Female	1.8 ± 0.3	1.6 ± 0.4	1.6 ± 0.4	1.5 ± 0.3	1.5 ± 0.4	1.4 ± 0.5
	Male	1.7 ± 0.4	1.6 ± 0.4	1.5 ± 0.4	1.5 ± 0.4	1.5 ± 0.3	1.6 ± 0.4
Homozygote	Female	1.6 ± 0.4	1.5 ± 0.4	1.4 ± 0.5	1.3 ± 0.4	1.3 ± 0.5	1.1 ± 0.4
	Male	1.6 ± 0.1	1.5 ± 0.3	1.4 ± 0.2	1.2 ± 0.3	1.3 ± 0.2	1.3 ± 0.2
Anterior-posterior width [mm]		C1	C2	C3	C4	C5	C6
NTL	Female	1.6 ± 0.3	1.5 ± 0.2	1.4 ± 0.2	1.4 ± 0.2	1.4 ± 0.2	1.5 ± 0.2
	Male	1.6 ± 0.3	1.5 ± 0.2	1.5 ± 0.2	1.4 ± 0.2	1.4 ± 0.2	1.3 ± 0.3
Hemizygote	Female	1.6 ± 0.3	1.5 ± 0.2	1.4 ± 0.2	1.4 ± 0.2	1.4 ± 0.2	1.4 ± 0.2
	Male	1.6 ± 0.4	1.5 ± 0.2	1.5 ± 0.2	1.5 ± 0.2	1.4 ± 0.2	1.4 ± 0.2
Homozygote	Female	1.4 ± 0.2	1.3 ± 0.3	1.3 ± 0.3	1.2 ± 0.3	1.2 ± 0.3	1.2 ± 0.3
	Male	1.4 ± 0.2	1.4 ± 0.2	1.4 ± 0.2	1.3 ± 0.2	1.3 ± 0.2	1.3 ± 0.2
Left-right width [mm]		C1	C2	C3	C4	C5	C6
NTL	Female	2.3 ± 0.4	2.2 ± 0.5	2.2 ± 0.5	2.2 ± 0.5	2.2 ± 0.5	2.2 ± 0.5
	Male	2.2 ± 0.3	2.2 ± 0.4	2.1 ± 0.3	2.1 ± 0.3	2.0 ± 0.3	1.9 ± 0.2
Hemizygote	Female	2.5 ± 0.2	2.4 ± 0.3	2.3 ± 0.4	2.2 ± 0.3	2.3 ± 0.3	2.2 ± 0.4
	Male	2.4 ± 0.3	2.3 ± 0.3	2.3 ± 0.2	2.3 ± 0.3	2.2 ± 0.3	2.3 ± 0.3
Homozygote	Female	2.1 ± 0.4	2.0 ± 0.4	2.0 ± 0.5	1.9 ± 0.5	1.9 ± 0.5	1.8 ± 0.5
	Male	2.2 ± 0.2	2.1 ± 0.2	2.1 ± 0.2	2.1 ± 0.3	2.2 ± 0.3	2.1 ± 0.3

NTL, non-transgenic littermates.

with a difference of the mean = 0.473, $t = 3.402$, $p = 0.002$, where values were found reduced (Table 3). No differences were found between hemizygous mice and non-transgenic littermates, with a difference of the mean = 0.104, $t = 0.797$, $p = 0.426$.

Analysis of the factor genotype between male animals revealed no significant difference between homozygous P301L mice and non-transgenic littermates, with a difference of the mean = 0.067, $t = 0.499$, $p = 0.618$. Similarly, there was no statistically significant difference between homozygous and hemizygous P301L mice, with a difference of the mean = 0.278, $t = 2.065$, $p = 0.115$; and there was no significant difference between hemizygous P301L mice and non-transgenic littermates, with a difference of the mean = 0.210, $t = 1.567$, $p = 0.223$.

Effect of Tau Pathology on Cervical Gray Matter Area

Statistical analysis of gray matter area between age-matched hemizygous, homozygous P301L mice, and non-transgenic

littermates revealed a two-way interaction between genotype and gender, $F_{(2)} = 8.263$, $p < 0.001$ (Tables 2, 3). Subsequent analysis of the factor genotype between female animals revealed a significant difference between homozygous P301L mice and non-transgenic littermates, with a difference of the mean = 0.387, $t = 4.934$, $p < 0.001$. Cross-sectional areas were decreased in homozygous P301L compared to non-transgenic littermates (Table 3). A significant difference was also observed between homozygous and hemizygous P301L mice, with a difference of the mean = 0.268, $t = 3.326$, $p = 0.002$, with a decrease in values (Table 3). No differences were found between hemizygous mice and non-transgenic littermates, with a difference of the mean = 0.119, $t = 1.574$, $p = 0.117$.

Analysis of the factor genotype between male animals revealed no significant difference between homozygous P301L mice and non-transgenic littermates, with a difference of the mean = 0.0549, $t = 0.705$, $p = 0.482$. In addition, there was no statistically significant difference between homozygous and hemizygous P301L mice, with a difference of the mean = 0.103, $t = 1.321$, $p = 0.340$; and there was no significant difference

TABLE 3 | Comparison of morphometric measures.

	Change homozygote to NTL [%]		Change homozygote to hemizygote [%]		Change hemizygote to NTL [%]	
	Female	Male	Female	Male	Female	Male
Total cross-sectional area						
C1	-10.2*	-7.2	-13.6*	-12.0	3.9	5.5
C2	-16.5*	-7.2	-15.8*	-8.8	-0.9	1.8
C3	-21.0*	-6.1	-19.0*	-7.9	-2.5	1.9
C4	-18.5*	-1.3	-13.4*	-10.8	-6.0	10.6
C5	-24.0*	1.1	-17.9*	-7.8	-7.4	9.6
C6	-31.3*	10.0	-23.7*	-9.2	-9.9	21.1
Gray matter area						
C1	-19.5*	-8.0	-20.6*	-17.8	1.4	11.9
C2	-26.9*	-3.9	-23.4*	-12.4	-4.5	9.7
C3	-31.8*	0	-27.7*	-8.2	-5.6	8.9
C4	-26.1*	13.9	-15.0*	-3.2	-13.1	17.7
C5	-37.5*	10.7	-23.4*	-1.5	-18.4	12.4
C6	-34.1*	23.5	-22.7*	3.0	-14.7	19.9
White matter area						
C1	-2.2	-6.2	-7.8	-5.8	6.0	-0.3
C2	-7.8	-12.3	-9.8	-8.2	2.3	-4.4
C3	-11.9	-10.8	-12.1	-7.5	0.2	-3.6
C4	-12.0	-13.7	-12.2	-17.8	0.3	4.9
C5	-11.6	-6.3	-13.9	-12.8	2.7	7.4
C6	-29.0	-0.2	-24.4	-18.2	-6.0	22.1
Anterior-posterior width						
C1	-12.0	-11.7	-12.0	-12.0	0	0.4
C2	-14.9	-7.6	-14.9	-10.1	0	2.8
C3	-11.3	-6.7	-11.3	-4.3	0	-2.4
C4	-10.6	-3.1	-10.6	-8.8	0	6.3
C5	-11.3	-3.0	-11.3	-7.6	0	5.1
C6	-21.4	1.3	-15.2	-7.3	-7.3	9.3
Left-right width						
C1	-8.7*	-3.3	-17.1*	-8.7	10.2	6.0
C2	-8.8*	-4.5	-14.6*	-7.9	6.8	3.7
C3	-8.8*	-1.7	-12.6*	-9.4	4.4	8.4
C4	-16.0*	1.4	-15.9*	-7.8	-0.2	10.0
C5	-11.8*	6.9	-15.0*	-1.5	3.7	8.5
C6	-17.9*	9.9	-15.8*	-6.5	-2.5	17.5

NTL, non-transgenic littermates. *Indicates statistically significant differences between mice of a different genotype and same gender using a two-way ANOVA ($p < 0.05$).

between hemizygous P301L mice and non-transgenic littermates, with a difference of the mean = 0.158, $t = 2.025$, $p = 0.126$.

Effect of Tau Pathology on Cervical White Matter Area

Statistical analysis of white matter area between age-matched hemizygous, homozygous P301L mice, and non-transgenic littermates revealed no statistically significant two-way interaction between genotype and gender, $F_{(2)} = 0.178$, $p = 0.837$ (Tables 2, 3). Subsequent analysis showed no effect of gender, $F_{(1)} = 0.036$, $p = 0.846$. However, analysis demonstrated an effect of genotype, $F_{(2)} = 7.554$, $p < 0.001$. Subsequent analysis of the factor genotype revealed a significant difference between homozygous P301L mice and non-transgenic littermates, with a difference of the mean = 0.159, $t = 3.051$, $p < 0.005$. A significant difference was also observed between homozygous and hemizygous P301L mice, with a difference of the mean = 0.193, $t = 3.650$, $p < 0.001$. No differences were found between hemizygous mice and non-transgenic littermates, with a difference of the mean = 0.034, $t = 0.661$, $p = 0.509$.

Effect of Tau Pathology on Anterior-Posterior and Left-Right Width

Statistical analysis of the anterior-posterior width between age-matched hemizygous, homozygous P301L mice, and non-transgenic littermates revealed no statistically significant two-way interaction between genotype and gender, $F_{(2)} = 1.471$, $p = 0.232$ (Tables 2, 3). Subsequent analysis showed no effect of gender, $F_{(1)} = 2.670$, $p = 0.103$. However, analysis demonstrated an effect of genotype, $F_{(2)} = 11.823$, $p < 0.001$. Subsequent analysis of the factor genotype revealed a significant difference between homozygous P301L mice and non-transgenic littermates, with a difference of the mean = 0.136, $t = 3.998$, $p < 0.001$. A significant difference was also observed between homozygous and hemizygous P301L mice, with a difference of the mean = 0.154, $t = 4.453$, $p < 0.001$. No differences were found between hemizygous mice and non-transgenic littermates, with a difference of the mean = 0.0176, $t = 0.526$, $p = 0.599$.

Statistical analysis of left-right width revealed a two-way interaction between genotype and gender, $F_{(2)} = 4.144$, $p < 0.017$ (Tables 2, 3). Subsequent analysis of the factor

genotype between female animals revealed a significant difference between homozygous P301L mice and non-transgenic littermates, with a difference of the mean = 0.268, $t = 3.676$, $p < 0.001$. Anterior-posterior widths were decreased in homozygous P301L compared to non-transgenic littermates (**Table 3**). A significant difference was also observed between homozygous and hemizygous P301L mice, with a difference of the mean = 0.352, $t = 4.701$, $p < 0.001$, with a decrease in values (**Table 3**). No differences were found between hemizygous mice and non-transgenic littermates, with a difference of the mean = 0.084, $t = 1.195$, $p = 0.233$.

Analysis of the factor genotype between male animals revealed no significant difference between homozygous P301L mice and non-transgenic littermates, with a difference of the mean = 0.0248, $t = 0.343$, $p = 0.732$. In addition, there was no statistically significant difference between homozygous and hemizygous P301L mice, with a difference of the mean = 0.161, $t = 2.226$, $p = 0.053$. There was a significant difference between hemizygous P301L mice and non-transgenic littermates, with a difference of the mean = 0.186, $t = 2.569$, $p = 0.032$.

Marked Neurodegeneration and Neuroinflammation in the Gray Matter of the Cervical SC

Immunohistochemical analysis revealed marked differences in NeuN and Iba-1 stainings between NTLs and hemizygous and homozygous P301L mice (**Figure 3**). Quantification of stainings showed reduced gray matter areas in the cervical SCs from P301L homozygous animals compared to hemizygous P301L mice and NTLs (**Figure 3B**). Similarly, the expression of the neuronal marker NeuN was reduced in P301L homozygous animals compared to hemizygous P301L mice and NTLs, while hemizygous P301L mice displayed higher NeuN levels than NTL. White matter areas were reduced in homozygous P301L compared to hemizygous littermates. Neuroinflammation was evident by increased Iba-1 staining in homozygous P301L mice compared to hemizygous littermates and NTLs.

DISCUSSION

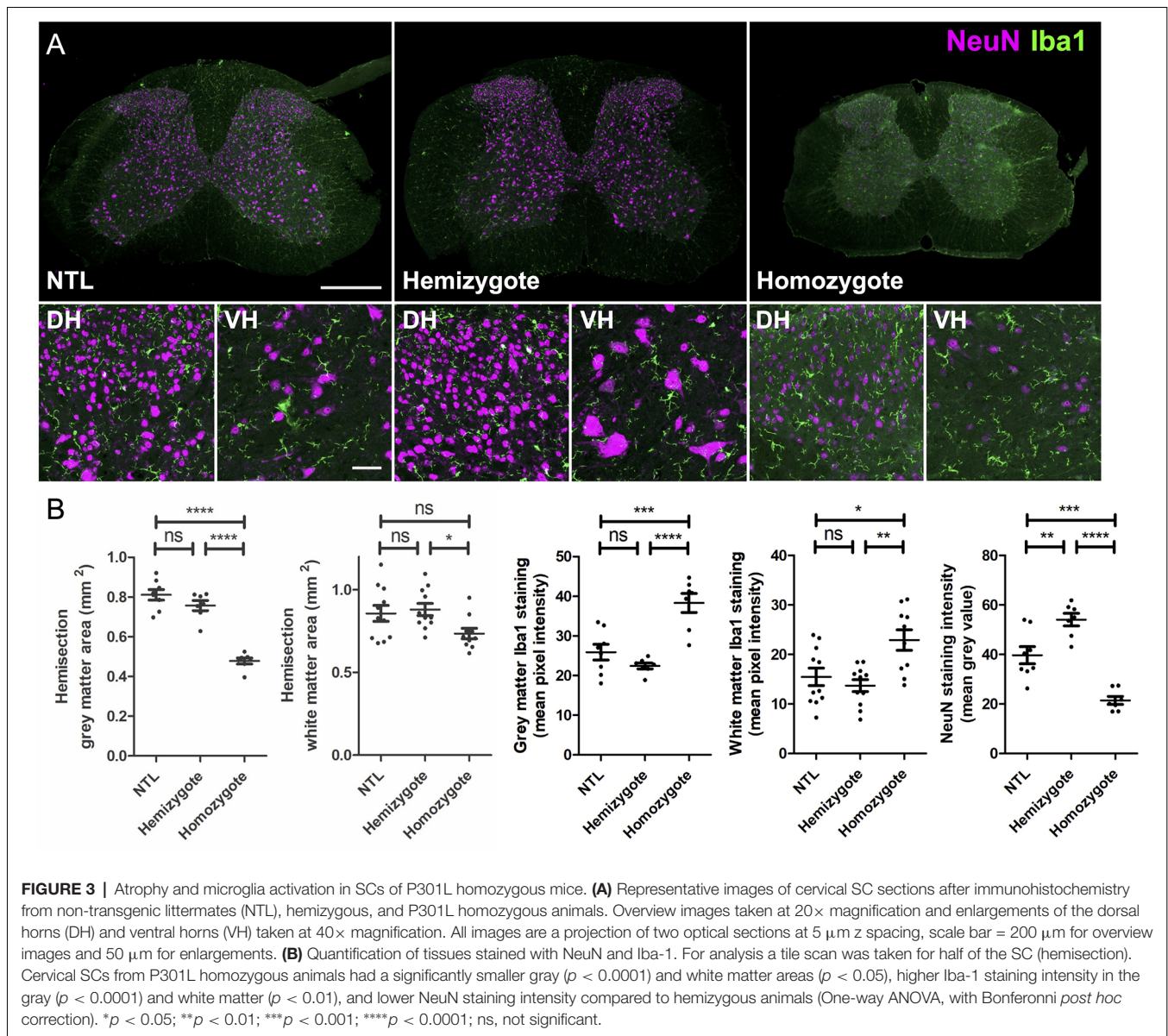
We characterized morphological changes of the cervical SC in the P301L mouse model of tauopathy. Computing morphometric metrics from structural high-resolution *ex vivo* MRI data revealed atrophy of the cervical segments C1–6. Importantly, we found that the observed changes depend both on gender and transgene expression levels. Immunohistochemical analysis revealed atrophy in conjunction with neuroinflammation in the cervical SC of P301L mice.

Structural MRI has been used to assess morphology of the normal SC in humans (Sherman et al., 1990; Kato et al., 2012; Engl et al., 2013; Ulbrich et al., 2014; Papinutto et al., 2015), but values for the mouse cervical SC have so far not been reported. Thus, we first determined morphometric metrics of the cervical SC in non-transgenic littermates (**Figure 2, Table 2**). Cross-sectional area, gray matter and white matter areas as well as anterior-posterior and left-right widths followed the described

anatomical structure of the cervical SC (Sengul and Watson, 2012). Human MRI studies have suggested sexual dimorphism of the cervical total cross-sectional, gray and white matter areas in adults, with men having larger values compared to women (Ulbrich et al., 2014; Papinutto et al., 2015). It has been suggested that this difference reflects differences in size between genders as SC measures are highly correlated with total cranial volume and vertebral dimensions (Papinutto et al., 2015). However, other studies have not seen differences in morphometric measures between males and females (Sherman et al., 1990; Kato et al., 2012; Engl et al., 2013). In our study, we did not observe significant differences in any of the analyzed morphometric measures between male and female non-transgenic mice. Male mice of the C57Bl6 background are heavier than females (Kovács and Pearce, 2013), which however was unrelated to higher morphometric measures in cervical cord. However, the small group sizes, compared to clinical MRI SC studies, might have prevented us from detecting a sexual dimorphism in cervical SC measures. More systematic studies assessing morphometric measures in male and female mice in larger cohorts should be conducted.

We further characterized morphological changes of the cervical SC related to tau by comparing morphometric metrics of hemizygous and homozygous P301L mice with age-matched non-transgenic littermates. We found clear evidence for atrophy of the cervical SC in P301L mice (**Table 3**). Thus, we further determined how gender, transgene expression, and anatomical location are related to the observed changes in cervical SC morphology.

While we have not seen an effect of gender in the normal morphology of the cervical SC, we tested for gender differences in tau-related cervical SC atrophy. Gender effects have been reported in the manifestation and progression of a variety of neurological diseases such as stroke (Cordonnier et al., 2017), Parkinson's disease (Liu et al., 2017), and SC injury (Stewart et al., 2020). Gender differences have also been reported for tauopathies. In Alzheimer's disease there is not only a higher prevalence in women than men (Plassman et al., 2007; Carter et al., 2012), but it is also associated with a higher tau cerebrospinal fluid level, cortical tau load, and degree of neurodegeneration in females (Filon et al., 2016; Hohman et al., 2018). Moreover, neuroimaging studies in cognitively normal adults and patients with mild cognitive impairment have shown that women exhibit higher cerebral tau accumulation than men, and a different spread of tau pathology across the brain (Buckley et al., 2019; Shokouhi et al., 2020). Sexual dimorphism of the observed phenotype in animal models of tauopathy is not consistently assessed. Specifically, the results from the small number of studies examining the effect of gender vary considerably. A study using rTg4510 mice showed significantly higher levels of hyperphosphorylated tau in females than males, associated with more severe impairment in spatial learning and memory (Yue et al., 2011). In contrast, a study in P301S showed a stronger cognitive deficit, neuropathology, and inflammatory plasma proteins in male transgenic mice (Sun et al., 2020). We have recently reported no differences in the number of cerebral calcifications between male and female P301L mice as observed



with susceptibility weighted imaging and phase imaging (Ni et al., 2020). In the present study, we observed a statistically significant two-interaction between genotype and gender for total cross-sectional area, gray matter area and left-right width where subsequent analysis revealed significant differences in this parameter for female mice only (Table 3). No two-way interaction was found for the white matter area and anterior-posterior width. This clearly implicates gender as an important factor in the observed phenotype of cervical SC atrophy.

We have also studied the effect of transgene-dosing on the measured morphometric measures by including both hemizygous and homozygous P301L mice in the study. In a recent brain diffusion tensor imaging study, we found more pronounced and wide-spread microstructural changes in homozygous compared to hemizygous P301L mice

(Massalimova et al., 2020). In this study, we observed stronger reduction in total cross-sectional area, and gray and white matter areas in homozygous than in hemizygous P301L mice (Table 3). For anterior-posterior and left-right width there was no obvious differences in the measured reductions between hemizygote and homozygote mice compared to non-transgenic littermates (Table 3). These observations are in line with immunohistochemical analysis, where we have seen lower gray and white matter as well as lower NeuN staining intensities in homozygous P301L mice compared to their hemizygous littermates and NTLs, while there was no difference between these measures in hemizygous P301L mice compared to NTL (Figure 3). Taken together the data shows that high transgene overexpression is a second important contributor to the observed phenotype.

Another aspect constitutes the location of neuropathology in the SC. A neuropathological study in Alzheimer's disease patients suggested a gradient in the SC tau pathology, with more pronounced tau deposition in the cervical SC, which decreased progressively from the thoracic to the lumbar level (Dugger et al., 2013). In the present study, we have only acquired data from the cervical SC segments C1 to C6 as this area was covered by the birdcage coil. Thus, we have no information about SC morphometric measures for the lowest cervical segments (C7 and C8) as well as the more distal parts of the SC. In the cervical region (C1-C6) we have seen decreases in total cross-sectional area, and gray and white matter area across all segments (Table 3). This is line with a recent study in Alzheimer's disease patients, which found reduced cross-sectional areas in segments C1 to C5 (Lorenzi et al., 2020). Thus, further studies should aim to elucidate the relationship between morphometric measures in the SC and tau pathology in other SC regions and assess how cervical SC atrophy progresses during the disease course. Moreover, structural MRI studies have shown regional atrophy in the brain of patients with tauopathies (Lieberman et al., 1998; Price et al., 2004; Ghetti et al., 2008; Holland et al., 2009; Shi et al., 2009; Tokumaru et al., 2009; Rohrer et al., 2010; Tabatabaei-Jafari et al., 2019; Lorenzi et al., 2020). Cerebral atrophy was also seen in preclinical MRI studies of mouse models of tauopathy (Xie et al., 2010; Yue et al., 2011; Holmes et al., 2017; Ma et al., 2019). In a recent study, we have not seen cerebral atrophy in hemizygous P301L mice at 10–12 and 19–21 months of age (Kindler et al., 2021), but we have not yet studied cerebral morphology in homozygous P301L mice. As the observation of cervical SC atrophy is a novel finding, the relationship between cerebral and cervical SC atrophy in models of tauopathy needs to be further investigated.

Neuropathological studies in the SC have shown that the tau pathology affects both gray and white matter (Ishihara et al., 1999; Spittaels et al., 1999; Probst et al., 2000; Verkkoniemi et al., 2001; Allen et al., 2002; Higuchi et al., 2002; Zehr et al., 2004; Lin et al., 2005; Rudzinski et al., 2008; Dugger et al., 2013). While we have seen also reductions in the white matter area in homozygous and hemizygous P301L mice compared to non-transgenic littermates, reductions were stronger in the gray matter (Table 3). This is in agreement with immunohistochemical analysis where we have seen significant reductions in the white matter area in homozygous P301L mice compared to hemizygous P301L mice and NTLs, but the reductions in gray matter area were more pronounced (Figure 3). This suggests that the overall observed atrophy in the cervical SC is largely due to degeneration of the gray matter. We have also observed that the degenerative changes were accompanied by inflammation, as shown by increased Iba-1 expression in the gray and white matter in homozygous P301L mice (Figure 3), confirming previous reports in different mouse tauopathy mouse models (Allen et al., 2002; Higuchi et al., 2002; Lin et al., 2005; Yoshiyama et al., 2007; Rudzinski et al., 2008).

In this study, we acquired structural T₁-weighted data of the cervical SC *ex vivo*. *Ex vivo* MRI offers distinct advantages over *in vivo* MRI studies (Stroman et al., 2014).

First, the small size of mouse SC requires a high spatial resolution of the SC to reliably depict anatomical details. *Ex vivo* MRI allowed long data acquisition, which we used to achieve a 50 μm isotropic resolution with high signal-to-noise ratio. Second, motion of the SC and its surrounding tissue by breathing and cerebrospinal fluid flow can lead to motion artifacts during *in vivo* MRI acquisition, which does not occur in *ex vivo* acquisitions. Third, inhomogeneities in magnetic susceptibility from air-tissue interfaces, result in image distortions and a loss of signal intensity. Embedding samples in perfluoropolyether effectively eliminates air from around the sample. In similar preparations of the head, we have recently shown microstructural changes in the gray and white matter of the brain in P301L mice of the same age as used in the current study with diffusion tensor imaging (Massalimova et al., 2020) and cerebral calcifications with susceptibility weighted imaging and phase imaging (Ni et al., 2020). Future studies should aim to assess neurodegenerative changes in the cervical SC with MRI *in vivo*. Furthermore, advanced quantitative MRI protocols have been applied to the SC and have the potential to provide sensitive and specific markers of SC pathology (Seif et al., 2018). Such tools may help to improve the diagnosis, stratification, and monitoring of patients with tauopathies.

In summary, we provide evidence for cervical SC atrophy in P301L mice, that depends both on gender and transgene expression levels. Future MRI studies in mouse models of tauopathies should focus on the role of cervical SC in the disease progression and symptomatology.

DATA AVAILABILITY STATEMENT

The raw data supporting the conclusions of this article will be made available by the authors, without undue reservation.

ETHICS STATEMENT

The animal study was reviewed and approved by Cantonal Veterinary Office Zurich. Written informed consent was obtained from the owners for the participation of their animals in this study.

AUTHOR CONTRIBUTIONS

JK conceived and designed the study and wrote the manuscript. TS and RG performed the experiments. TS, RG, and JK analyzed the data. TS, RG, RN, PF, HZ, and JK interpreted the results. All authors contributed to the article and approved the submitted version.

FUNDING

JK received funding from the Olga Mayenfisch Stiftung. PF was funded by a Swiss National Science Foundation Eccellenza Professorial Fellowship grant (PCEFP3_181362/1).

REFERENCES

- Allen, B., Ingram, E., Takao, M., Smith, M. J., Jakes, R., Virdee, K., et al. (2002). Abundant tau filaments and nonapoptotic neurodegeneration in transgenic mice expressing human P301S tau protein. *J. Neurosci.* 22, 9340–9351. doi: 10.1523/JNEUROSCI.22-21-09340.2002
- Braak, H., and Braak, E. (1991). Neuropathological staging of Alzheimer-related changes. *Acta Neuropathol.* 82, 239–259. doi: 10.1007/BF00308809
- Buckley, R. F., Mormino, E. C., Rabin, J. S., Hohman, T. J., Landau, S., Hanseeuw, B. J., et al. (2019). Sex differences in the association of global amyloid and regional tau deposition measured by positron emission tomography in clinically normal older adults. *JAMA Neurol.* 76, 542–551. doi: 10.1001/jamaneurol.2018.4693
- Carter, C. L., Resnick, E. M., Mallampalli, M., and Kalbarczyk, A. (2012). Sex and gender differences in Alzheimer's disease: recommendations for future research. *J. Womens Health (Larchmt)* 21, 1018–1023. doi: 10.1089/jwh.2012.3789
- Cordonnier, C., Sprigg, N., Sandset, E. C., Pavlovic, A., Sunnerhagen, K. S., Caso, V., et al. (2017). Stroke in women—from evidence to inequalities. *Nat. Rev. Neurol.* 13, 521–532. doi: 10.1038/nrneurol.2017.95
- Duff, K., Knight, H., Refolo, L. M., Sanders, S., Yu, X., Picciano, M., et al. (2000). Characterization of pathology in transgenic mice over-expressing human genomic and cDNA tau transgenes. *Neurobiol. Dis.* 7, 87–98. doi: 10.1006/nbdi.1999.0279
- Dugger, B. N., Hidalgo, J. A., Chiarolanza, G., Mariner, M., Henry-Watson, J., Sue, L. I., et al. (2013). The distribution of phosphorylated tau in spinal cords of Alzheimer's disease and non-demented individuals. *J. Alzheimers Dis.* 34, 529–536. doi: 10.3233/JAD-121864
- Ellingson, B. M., Schmit, B. D., and Kurpad, S. N. (2010). Lesion growth and degeneration patterns measured using diffusion tensor 9.4-T magnetic resonance imaging in rat spinal cord injury: presented at the 2009 joint spine section meeting. *J. Neurosurg. Spine* 13, 181–192. doi: 10.3171/2010.3.SPINE09523
- Engl, C., Schmidt, P., Arsic, M., Boucard, C. C., Biberacher, V., Röttinger, M., et al. (2013). Brain size and white matter content of cerebrospinal tracts determine the upper cervical cord area: evidence from structural brain MRI. *Neuroradiology* 55, 963–970. doi: 10.1007/s00234-013-1204-3
- Filon, J. R., Intorcica, A. J., Sue, L. I., Vazquez Arreola, E., Wilson, J., Davis, K. J., et al. (2016). Gender differences in Alzheimer disease: brain atrophy, histopathology burden and cognition. *J. Neuropathol. Exp. Neurol.* 75, 748–754. doi: 10.1093/jnen/nlw047
- Ghetti, B., Spina, S., Murrell, J. R., Huey, E. D., Pietrini, P., Sweeney, B., et al. (2008). *In vivo* and postmortem clinicoanatomical correlations in frontotemporal dementia and parkinsonism linked to chromosome 17. *Neurodegener. Dis.* 5, 215–217. doi: 10.1159/000113706
- Götz, J., Chen, F., Barmettler, R., and Nitsch, R. M. (2001). Tau filament formation in transgenic mice expressing P301L tau. *J. Biol. Chem.* 276, 529–534. doi: 10.1074/jbc.M006531200
- Grundke-Iqbal, I., Iqbal, K., and Tung, Y. C. (1986). Abnormal phosphorylation of the microtubule-associated protein τ (tau) in Alzheimer cytoskeletal pathology. *Proc. Natl. Acad. Sci. U S A* 83, 44913–44917. doi: 10.1073/pnas.83.13.4913
- Higuchi, M., Ishihara, T., Zhang, B., Hong, M., Andreadis, A., Trojanowski, J. Q., et al. (2002). Transgenic mouse model of tauopathies with glial pathology and nervous system degeneration. *Neuron* 35, 433–446. doi: 10.1016/s0896-6273(02)00789-4
- Hohman, T. J., Dumitrescu, L., Barnes, L. L., Thambisetty, M., Beecham, G., Kunkle, B., et al. (2018). Sex-specific association of apolipoprotein e with cerebrospinal fluid levels of tau. *JAMA Neurol.* 75, 989–998. doi: 10.1001/jamaneurol.2018.0821
- Holland, D., Brewer, J. B., Hagler, D. J., Fennema-Notestine, C., and Dale, A. M. (2009). Subregional neuroanatomical change as a biomarker for Alzheimer's disease. *Proc. Natl. Acad. Sci. U S A* 106, 20954–20959. doi: 10.1073/pnas.0906053106
- Holmes, H. E., Powell, N. M., Ma, D., Ismail, O., Harrison, I. F., Wells, J. A., et al. (2017). Comparison of *in vivo* and *ex vivo* mri for the detection of structural abnormalities in a mouse model of tauopathy. *Front. Neuroinform.* 11:20. doi: 10.3389/fninf.2017.00020
- Iaccarino, L., Tammewar, G., Ayakta, N., Baker, S. L., Bejanin, A., Boxer, A. L., et al. (2018). Local and distant relationships between amyloid, tau and neurodegeneration in Alzheimer's disease. *Neuroimage Clin.* 17, 452–464. doi: 10.1016/j.nicl.2017.09.016
- Ishihara, T., Hong, M., Zhang, B., Nakagawa, Y., Lee, M. K., Trojanowski, J. Q., et al. (1999). Age-dependent emergence and progression of a tauopathy in transgenic mice overexpressing the shortest human tau isoform. *Neuron* 24, 751–762. doi: 10.1016/s0896-6273(00)81127-7
- Joie, R. L., Visani, A. V., Baker, S. L., Brown, J. A., Bourakova, V., Cha, J., et al. (2020). Prospective longitudinal atrophy in Alzheimer's disease correlates with the intensity and topography of baseline tau-PET. *Sci. Transl. Med.* 12:eaau5732. doi: 10.1126/scitranslmed.aau5732
- Josephs, K. A. (2017). Current understanding of neurodegenerative diseases associated with the protein tau. *Mayo Clin. Proc.* 92, 1291–1303. doi: 10.1016/j.mayocp.2017.04.016
- Kato, F., Yukawa, Y., Suda, K., Yamagata, M., and Ueta, T. (2012). Normal morphology, age-related changes and abnormal findings of the cervical spine. part II: magnetic resonance imaging of over 1,200 asymptomatic subjects. *Eur. Spine J.* 21, 1499–1507. doi: 10.1007/s00586-012-2176-4
- Kindler, D., Maschio, C., Ni, R., Zerbi, V., Razansky, D., and Klohs, J. (2021). Arterial spin labeling demonstrates preserved regional cerebral blood flow in the P301L mouse model of tauopathy. *J. Cereb. Blood Flow Metab.* 42, 686–693. doi: 10.1177/0271678X211062274
- Klohs, J., and Rudin, M. (2011). Unveiling molecular events in the brain by noninvasive imaging. *Neuroscientist* 17, 539–559. doi: 10.1177/1073858410383433
- Kovács, A. D., and Pearce, D. A. (2013). Location- and sex-specific differences in weight and motor coordination in two commonly used mouse strains. *Sci. Rep.* 3:2116. doi: 10.1038/srep02116
- Lee, V. M.-Y., Goedert, M., and Trojanowski, J. Q. (2001). Neurodegenerative tauopathies. *Annu. Rev. Neurosci.* 24, 1121–1159. doi: 10.1146/annurev.neuro.24.1.1121
- Lieberman, A. P., Trojanowski, J. Q., Lee, V. M. Y., Balin, B. J., Ding, X. S., Greenberg, J., et al. (1998). Cognitive, neuroimaging and pathological studies in a patient with Pick's disease. *Ann. Neurol.* 43, 259–265. doi: 10.1002/ana.410430218
- Lin, W. L., Lewis, J., Yen, S. H., Hutton, M., and Dickson, D. W. (2003). Ultrastructural neuronal pathology in transgenic mice expressing mutant (P301L) human tau. *J. Neurocytol.* 32, 1091–1105. doi: 10.1023/B:NEUR.0000021904.61387.95
- Lin, W.-L., Zehr, C., Lewis, J., Hutton, M., Yen, S.-H., and Dickson, D. W. (2005). Progressive white matter pathology in the spinal cord of transgenic mice expressing mutant (P301L) human tau. *J. Neurocytol.* 34, 397–410. doi: 10.1007/s11068-006-8726-0
- Liu, G., Locascio, J. J., Corvol, J. C., Boot, B., Liao, Z., Page, K., et al. (2017). Prediction of cognition in Parkinson's disease with a clinical-genetic score: a longitudinal analysis of nine cohorts. *Lancet Neurol.* 16, 620–629. doi: 10.1016/S1474-4422(17)30122-9
- Lorenzi, R. M., Palesi, F., Castellazzi, G., Vitali, P., Anzalone, N., Bernini, S., et al. (2020). Unsuspected involvement of spinal cord in Alzheimer disease. *Front. Cell. Neurosci.* 14:6. doi: 10.3389/fncel.2020.00006
- Ma, D., Holmes, H. E., Cardoso, M. J., Modat, M., and Harrison, I. F. (2019). Study the longitudinal *in vivo* and cross-sectional *ex vivo* brain volume difference for disease progression and treatment effect on mouse model of tauopathy using automated MRI structural parcellation. *Front. Neurosci.* 13:11. doi: 10.3389/fnins.2019.00011
- Mann, R. S., Constantinescu, C. S., and Tench, C. R. (2007). Upper cervical spinal cord cross-sectional area in relapsing remitting multiple sclerosis: application of a new technique for measuring cross-sectional area on magnetic resonance images. *J. Magn. Reson. Imaging* 26, 61–65. doi: 10.1002/jmri.20959
- Massalimova, A., Ni, R., Nitsch, R. M., Reiser, M., von Elverfeldt, D., and Klohs, J. (2020). Diffusion tensor imaging reveals whole-brain microstructural changes in the P301L mouse model of tauopathy. *Neurodegener. Dis.* 20, 173–184. doi: 10.1159/000515754
- Ni, R., Zarb, Y., Kuhn, G. A., Müller, R., Yundung, Y., Nitsch, R. M., et al. (2020). SWI and phase imaging reveal intracranial calcifications in the P301L mouse model of human tauopathy. *MAGMA* 33, 769–781. doi: 10.1007/s10334-020-00855-3

- Papinutto, N., Schlaeger, R., Panara, V., Zhu, A. H., Caverzasi, E., Stern, W. A., et al. (2015). Age, gender and normalization covariates for spinal cord gray matter and total cross-sectional areas at cervical and thoracic levels: a 2D phase sensitive inversion recovery imaging study. *PLoS One* 10:e0118576. doi: 10.1371/journal.pone.0118576
- Plassman, B. L., Langa, K. M., Fisher, G. G., Heeringa, S. G., Weir, D. R., Ofstedal, M. B., et al. (2007). Prevalence of dementia in the United States: the aging, demographics and memory study. *Neuroepidemiology* 29, 125–132. doi: 10.1159/000109998
- Price, S., Paviour, D., Schill, R., Stevens, J., Rossor, M., Lees, A., et al. (2004). Voxel-based morphometry detects patterns of atrophy that help differentiate progressive supranuclear palsy and Parkinson's disease. *Neuroimage* 23, 663–669. doi: 10.1016/j.neuroimage.2004.06.013
- Probst, A., Götz, J., Wiederhold, K. H., Tolnay, M., Mistl, C., Jaton, A. L., et al. (2000). Axonopathy and amyotrophy in mice transgenic for human four-repeat tau protein. *Acta Neuropathol.* 99, 469–481. doi: 10.1007/s004010051148
- Rohrer, J. D., Ridgway, G. R., Modat, M., Ourselin, S., Mead, S., Fox, N. C., et al. (2010). Distinct profiles of brain atrophy in frontotemporal lobar degeneration caused by progranulin and tau mutations. *Neuroimage* 53, 1070–1076. doi: 10.1016/j.neuroimage.2009.12.088
- Rosset, A., Spadola, L., and Ratib, O. (2004). OsiriX: an open-source software for navigating in multidimensional DICOM images. *J. Digit. Imaging* 17, 205–216. doi: 10.1007/s10278-004-1014-6
- Rudzinski, L. A., Fletcher, R. M., Dickson, D. W., Crook, R., Hutton, M. L., Adamson, J., et al. (2008). Early onset familial Alzheimer disease with spastic paraparesis, dysarthria and seizures and N135S mutation in PSEN1. *Alzheimer Dis. Assoc. Disord.* 22, 299–307. doi: 10.1097/WAD.0b013e3181732399
- Scarmeas, N., Albert, M., Brandt, J., Blacker, D., Hadjigeorgiou, G., Papadimitriou, A., et al. (2005). Motor signs predict poor outcomes in Alzheimer disease. *Neurology* 64, 1696–1703. doi: 10.1212/01.WNL.0000162054.15428.E9
- Schmidt, M. L., Zhukareva, V., Perl, D. P., Sheridan, S. K., Schuck, T., Lee, V. M. Y., et al. (2001). Spinal cord neurofibrillary pathology in Alzheimer disease and Guam parkinsonism-dementia complex. *J. Neuropathol. Exp. Neurol.* 60, 1075–1086. doi: 10.1093/jnen/60.11.1075
- Seif, M., Curt, A., Thompson, A. J., Grabher, P., Weiskopf, N., and Freund, P. (2018). Quantitative MRI of rostral spinal cord and brain regions is predictive of functional recovery in acute spinal cord injury. *Neuroimage Clin.* 20, 556–563. doi: 10.1016/j.nicl.2018.08.026
- Sengul, G., and Watson, C. (2012). "Spinal cord" in *The Mouse Nervous System*, eds C. Watson, G. Paxinos, and L. Puelles (Academic Press), 424–458.
- Sherman, J. L., Nassaux, P. Y., and Citrin, C. M. (1990). Measurements of the normal cervical spinal cord on MR imaging. *Am. J. Neuroradiol.* 11, 369–372.
- Shi, F., Liu, B., Zhou, Y., Yu, C., and Jiang, T. (2009). Hippocampal volume and asymmetry in mild cognitive impairment and Alzheimer's disease: meta-analyses of MRI studies. *Hippocampus* 19, 1055–1064. doi: 10.1002/hipo.20573
- Shokouhi, S., Taylor, W. D., Albert, K., Kang, H., and Newhouse, P. A. (2020). *In vivo* network models identify sex differences in the spread of tau pathology across the brain. *Alzheimers Dement. (Amst)* 12:e12016. doi: 10.1002/dad2.12016
- Spittaels, K., Van Den Haute, C., Van Dorpe, J., Bruynseels, K., Vandezande, K., Laenen, I., et al. (1999). Prominent axonopathy in the brain and spinal cord of transgenic mice overexpressing four-repeat human tau protein. *Am. J. Pathol.* 155, 2153–2165. doi: 10.1016/S0002-9440(10)65533-2
- Stewart, A. N., MacLean, S. M., Stromberg, A. J., Whelan, J. P., Bailey, W. M., Gensel, J. C., et al. (2020). Considerations for studying sex as a biological variable in spinal cord injury. *Front. Neurol.* 11:802. doi: 10.3389/fneur.2020.00802
- Stroman, P. W., Wheeler-Kingshott, C., Bacon, M., Schwab, J. M., Bosma, R., Brooks, J., et al. (2014). The current state-of-the-art of spinal cord imaging: Methods. *Neuroimage* 84, 1070–1081. doi: 10.1016/j.neuroimage.2013.04.124
- Sun, Y., Guo, Y., Feng, X., Jia, M., Ai, N., Dong, Y., et al. (2020). The behavioural and neuropathologic sexual dimorphism and absence of MIP-3α in tau P301S mouse model of Alzheimer's disease. *J. Neuroinflammation* 17:72. doi: 10.1186/s12974-020-01749-w
- Tabatabaei-Jafari, H., Shaw, M. E., Walsh, E., and Cherbuin, N. (2019). Regional brain atrophy predicts time to conversion to Alzheimer's disease, dependent on baseline volume. *Neurobiol. Aging* 83, 86–94. doi: 10.1016/j.neurobiolaging.2019.08.033
- Tokumaru, A. M., Saito, Y., Murayama, S., Kazutomi, K., Sakiyama, Y., Toyoda, M., et al. (2009). Imaging-pathologic correlation in corticobasal degeneration. *Am. J. Neuroradiol.* 30, 1884–1892. doi: 10.3174/ajnr.A1721
- Ulbrich, E. J., Schraner, C., Boesch, C., Hodler, J., Busato, A., Anderson, S. E., et al. (2014). Normative MR cervical spinal canal dimensions. *Radiology* 271, 172–182. doi: 10.1148/radiol.13120370
- Verkkoniemi, A., Kalimo, H., Paetau, A., Somer, M., Iwatsubo, T., Hardy, J., et al. (2001). Variant Alzheimer disease with spastic paraparesis: neuropathological phenotype. *J. Neuropathol. Exp. Neurol.* 60, 483–492. doi: 10.1093/jnen/60.5.483
- Vogel, J. W., Iturria-Medina, Y., Strandberg, O. T., Smith, R., Levitis, E., Evans, A. C., et al. (2020). Spread of pathological tau proteins through communicating neurons in human Alzheimer's disease. *Nat. Commun.* 11:2612. doi: 10.1038/s41467-020-15701-2
- Waite, L. M., Grayson, D. A., Piguet, O., Creasey, H., Bennett, H. P., and Broe, G. A. (2005). Gait slowing as a predictor of incident dementia: 6-year longitudinal data from the sydney older persons study. *J. Neurol. Sci.* 229–230, 89–93. doi: 10.1016/j.jns.2004.11.009
- Watson, C., Paxinos, G., Kayalioglu, G., and Heise, C. (2009). "Atlas of the mouse spinal cord," in *The Spinal Cord*, eds C. Watson, G. Paxinos, G. Kayalioglu, (San Diego, CA: Academic Press), 308–379. doi: 10.1016/B978-0-12-374247-6.50020-1
- Xie, Z., Yang, D., Stephenson, D., Morton, D., Hicks, C., Brown, T., et al. (2010). Characterizing the regional structural difference of the brain between tau transgenic (rTg4510) and wild-type mice using MRI. *Med. Image Comput. Comput. Assist. Interv.* 13, 308–315. doi: 10.1007/978-3-642-15705-9_38
- Yoshiyama, Y., Higuchi, M., Zhang, B., Huang, S. M., Iwata, N., Saido, T. C. C., et al. (2007). Synapse loss and microglial activation precede tangles in a P301S tauopathy mouse model. *Neuron* 53, 337–351. doi: 10.1016/j.neuron.2007.01.010
- Yue, M., Hanna, A., Wilson, J., Roder, H., and Janus, C. (2011). Sex difference in pathology and memory decline in rTg4510 mouse model of tauopathy. *Neurobiol. Aging* 32, 590–603. doi: 10.1016/j.neurobiolaging.2009.04.006
- Zehr, C., Lewis, J., McGowan, E., Crook, J., Lin, W. L., Godwin, K., et al. (2004). Apoptosis in oligodendrocytes is associated with axonal degeneration in P301L tau mice. *Neurobiol. Dis.* 15, 553–562. doi: 10.1016/j.nbd.2003.12.011

Conflict of Interest: The authors declare that the research was conducted in the absence of any commercial or financial relationships that could be construed as a potential conflict of interest.

Publisher's Note: All claims expressed in this article are solely those of the authors and do not necessarily represent those of their affiliated organizations, or those of the publisher, the editors and the reviewers. Any product that may be evaluated in this article, or claim that may be made by its manufacturer, is not guaranteed or endorsed by the publisher.

Copyright © 2022 Sartoretti, Ganley, Ni, Freund, Zeilhofer and Klohs. This is an open-access article distributed under the terms of the Creative Commons Attribution License (CC BY). The use, distribution or reproduction in other forums is permitted, provided the original author(s) and the copyright owner(s) are credited and that the original publication in this journal is cited, in accordance with accepted academic practice. No use, distribution or reproduction is permitted which does not comply with these terms.